Direct Laser Ablation of Glasses with Low Surface Roughness Using Femtosecond UV Laser Pulses

Dominyka Stonyte*, Vytautas Jukna, and Domas Paipulas*

Laser Research Center, Faculty of Physics, Vilnius University, Sauletekio av. 10, LT-10223 Vilnius, Lithuania

**Corresponding author's e-mail: dominyka.stonyte@ff.vu.lt, domas.paipulas@ff.vu.lt*

In this article, the properties of soda-lime glass after direct laser ablation are studied by utilizing femtosecond UV laser pulses of 206 nm wavelength, 300 fs duration at 50 kHz pulse repetition rate, generated by a solid-state Yb:KGW laser system. The results prove that linear light absorption allows the fabrication of good-quality pits with very low heat-affected zones (HAZ) without any post-processing. Several sets of pits were ablated with a varying number of laser pulses per spot and different pulse energies. Pits' width, depth, and volume parameter maps that show relations with the number of pulses per spot, laser pulse energy, and fluence are depicted. These maps are useful when considering a suitable set of parameters for the fabrication of diffractive optical or similar devices where low surface roughness is critical. The ablated craters were also inspected with a scanning electron microscope (SEM) which indicates that femtosecond UV laser pulses are capable to achieve a good quality ablation with a low surface roughness of the modified zone.

DOI: 10.2961/jlmn.2022.02.2008

Keywords: femtosecond, UV, laser ablation, micro structuring, multiple pulses, efficiency, low HAZ, high harmonics

1. Introduction

Direct laser ablation has always been a region of interest in the micro-processing field, where high precision is required. However, good quality fabrication of materials that are transparent to a laser wavelength has been quite a challenge in the past. Fortunately, recent advancements in industrial-grade systems, delivering ultrashort high-intensity femtosecond laser pulses made it possible to ablate even high bandgap materials [1].

Typical photon energies from a solid-state laser's first or second harmonic are not sufficient to induce linear absorption in almost all transparent materials, therefore only a nonlinear absorption mechanism can excite material's electrons to a conduction band and sustain the ablation process. Yet, the smoothest ablation results with low heat-affected zones (HAZ) are expected in the linear absorption regime. That is why UV lasers where the energy of photons is large enough for a linear absorption can lead to better results than using IR or visible spectrum [2]. Currently, most of the research in ablation with UV light is conducted usually with excimer lasers delivering longer nanosecond pulses [3,4]. For example, Y. T. Chen *et al.* [5] have ablated several different types of arrayed microstructures for various applications (optical waveguide, wave absorber, beam guider) on BK7 glass by using excimer ArF laser (λ = 193 nm, τ = 20 ns). Their results prove that excimer lasers can induce very localized and well-controlled energy absorption with minimized heat-affected zones.

Solid state lasers operating at UV wavelengths also show good results for the polishing of hard dielectric structures. In a recent study by H. Liu et al. [6] it was proved, that optical quality in laser polishing can be achieved with UV nanosecond pulses: they proposed the laser polishing process of a single-crystal chemical vapor deposition diamond using 355 nm, 25 ns pulses at a 50 kHz pulse repetition rate. The achieved minimum average roughness was below 9 nm and is much lower than the requirements of optical components at UV to IR wavelengths. Another promising study by Saliminia *et al.* [7] showed that strong Bragg gratings in pure silica photonic crystal fibers with up to 37 dB reflectivity can be inscribed by using femtosecond UV laser pulses and a Talbot interferometer. The usage of UV femtosecond laser pulses benefits from the lower irradiation intensities used because of higher nonlinear absorption in the glass. The optical filamentation of femtosecond laser pulses in silica glass was demonstrated as an accompanying process to the FBG writing. In addition, such direct writing technology is a very simple one-step process that does not require a clean room environment.

It is well known that shorter pulses have characteristic timescales much smaller than the material's atomic vibrations timescale and produce reduced HAZ which causes better ablation precision and quality if compared to longer pulses. For this reason, higher harmonics of solid-state femtosecond lasers could be a better choice if compared to excimer lasers.

In this study, we present femtosecond laser (206 nm, 50 kHz, 300 fs) ablation results on soda-lime glass. Single-spot ablation experiments were performed with Yb:KGW laser system (PHAROS Light Conversion) with 5th harmonic generator, Aerotech ANT180 micro-positioning system, and calcium fluoride lenses for beam focusing with

the focal length of 50 mm. The parametrical analysis of ablation outcome versus processing parameters is presented which indicates that UV machining can produce high-quality craters absent from HAZ without any additional post-processing.

2. Experimental setup

Our experimental setup is depicted in Fig. 1. As a light source, we used an ultrashort pulsed solid-state Yb:KGW laser system ("Pharos" "Light Conversion") with a 5th harmonic module. The system utilizes 206 nm wavelength 300 fs duration laser pulses at the repetition rate of 50 kHz. The laser light is directed by dielectric mirrors to the CaF_2 lens (50 mm focal length), which focuses light onto the sample's surface. The beam diameter in front of the lens was 0.61 mm ($2\omega_0$) and the sample surface was located slightly above (0.5 – 1 mm) geometrical focus in order to minimize intrinsic beam astigmatism effects that tend to destroy the gaussian shape beam profile. We have noticed that a slightly defocused laser beam has better symmetry and its diameter on the sample surface was measured to be 10.62 µm (Fig. 6).

Different ablation geometries are realized by moving the sample with "Aerotech ANT180" positioning stages in a horizontal plane (x, y directions). For precision, the velocity stabilization function was used where the stages accelerated for 2 mm before firing laser pulses. The lens is mounted on the vertical stage for the control of the focal position. The system automatization was carried out using the "DMC" (Direct Machining Control, Ltd.) software package. As there is a lack of commercially available attenuators for 206 nm wavelength, we attenuated laser power by inducing Fresnel losses from the several fused silica glass plates inserted in the beam path. After laser ablation, all samples were immersed in distilled water and cleaned in an ultrasonic bath for about 10 – 20 minutes.

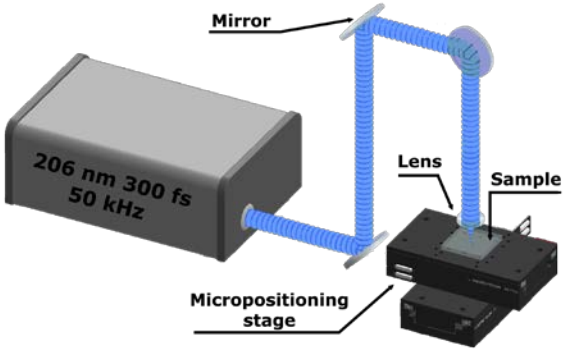

Fig. 1 Experimental setup.

For the evaluation of our results, we used an optical profilometer "Sensofar PLµ 2300" and a scanning electron microscope (SEM) "Thermo Fisher" "Prisma E". Ablation experiments were conducted on soda-lime glass.

3. Experimental ablation results and discussion

In this section, we discuss the results of crater formation by firing multiple laser pulses on the same spot on soda-lime glass. Here we will detail data analysis steps and provide fabrication parameter maps for achieving differing depth, width, volume, and ablation efficiency values as well as SEM images of selected craters.

The experiment of ablation by multiple pulses was performed by firing a varying amount of laser pulses to the same location for different laser average powers at a 50 kHz laser pulse repetition rate. All of the ablated craters were then measured with an optical profilometer and the data was processed using the "Matlab" software package. From every crater's 3D profilometer picture we correct the measurement errors, extract profiles across the craters' center and calculate the depth and width of the ablated pit. We define the depth of craters by the distance from the deepest point to the flat sample surface. We also calculate the exact volume of an ablated material from the 3D topography without making any theoretical assumptions about its shape.

The depth dependence on the number of pulses per spot is depicted in Fig. 2.

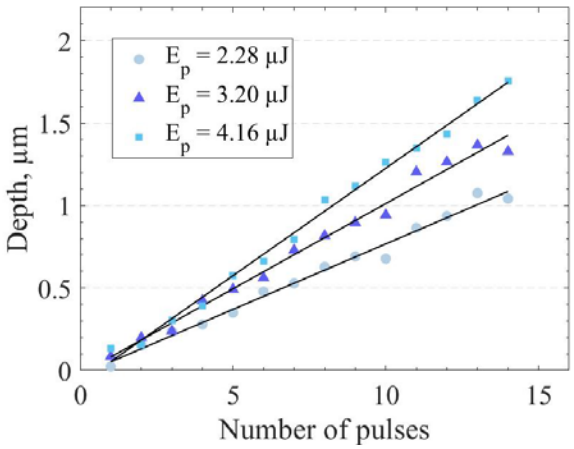

Fig. 2 Depth dependence on the number of pulses per spot.

Fig. 2 clearly shows linear depth dependence on the number of pulses. It means that each pulse with specific energy contributes equally to the ablation depth and saturation effects are not yet present till 15 shots. Naturally, the depth change with a continuous increase of the number of pulses will deviate from linear dependence as crater shape will start to influence laser absorption and lead to saturation [8, 9].

The volume dependence on the number of pulses per spot is depicted in Fig. 3.

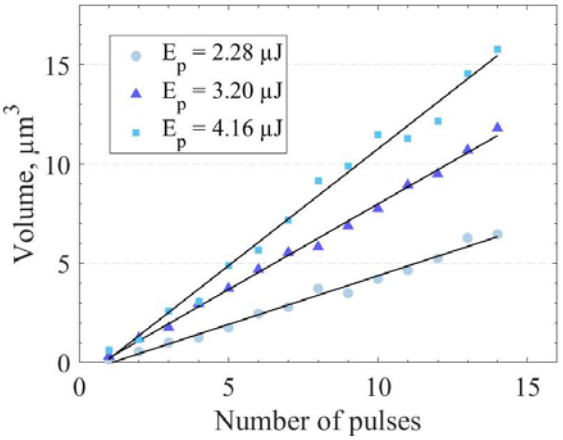

Fig. 3 Volume dependence on the number of pulses per spot.

It also shows the linear behavior of the number of pulses for all the averaged powers we have used. In contrast, the

width and efficiency dependencies are not linear and the saturation effect is clearly visible. The width and efficiency dependencies on the number of laser pulses, depicted respectively in Figs. 4-5 were fitted with a function ax^b+c , where a, b, and c are constants and x = N.

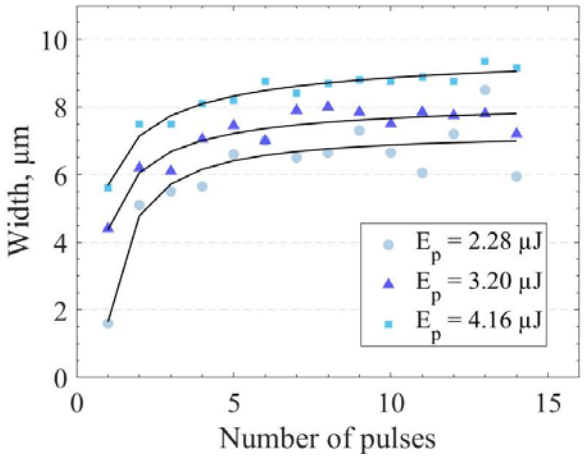

Fig. 4 Width dependence on the number of pulses per spot.

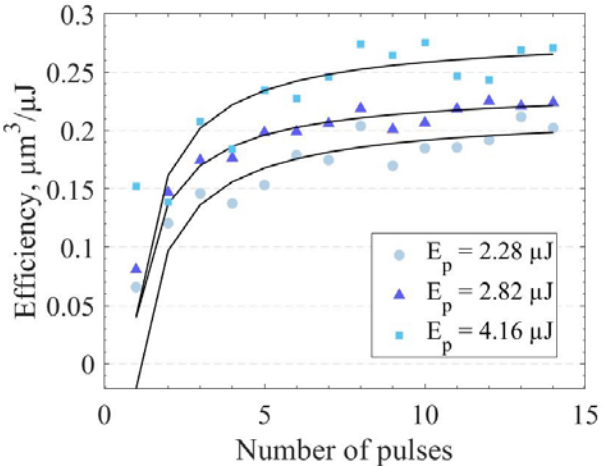

Fig. 5 Efficiency dependence on the number of pulses per spot.

The ablation efficiency was also calculated as $\eta = \frac{V}{E_p N}$, where E_p is energy in a single pulse, N – the number of pulses per spot, V – ablated volume. Here the pulse energy was calculated using the equation: $E_p = \frac{P_{avg}}{f_{rep}}$, where P_{avg} is the average power, measured by a power meter, and f_{rep} is a pulse repetition rate (50 kHz). The peak fluence was estimated using the standard gaussian beam equation: $F_0 = \frac{2E_p}{\pi\omega_0^2}$, where ω_0 is the beam radius on the sample, which can be experimentally found by scaling the diameter of the ablated craters D versus laser pulse energy E_p as: $D^2 = 2\omega_0^2 \ln(E_p)$ [10]. This is done in Fig. 6 which shows that our beam radius at the sample surface was 5.3 μm. The energy value where linear fit crosse the abscise axis gives an ablation threshold energy, which corresponds to the threshold fluence of 4.97 J/cm^2.

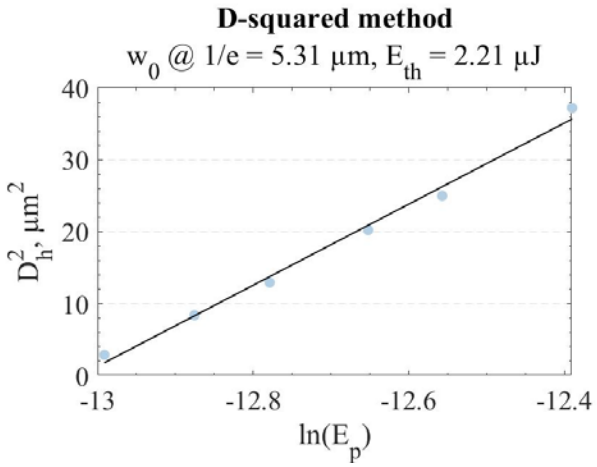

Fig. 6 Beam radius and ablation threshold energy calculation.

The experiment was performed with 7 different laser pulse energies. For each energy, the set of pits was ablated with a different amount of laser pulses, fired at the same spot. The depth of the craters' dependence on the number of pulses per spot and one pulse energy is depicted in Fig. 7.

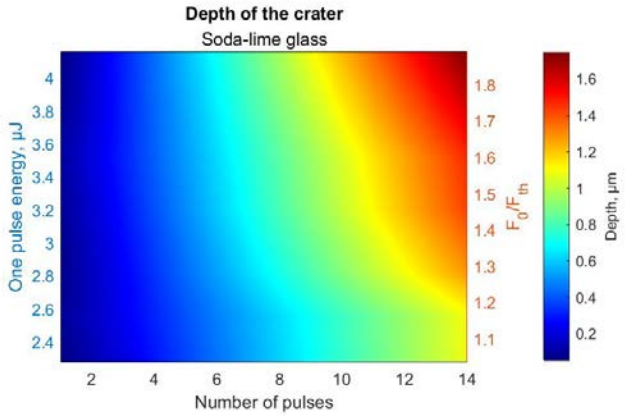

Fig. 7 Depth of the craters, ablated on soda-lime glass.

As was shown before, depth linearly depends on the number of laser pulses for each pulse energy, but depth dependence on pulse energy is not linear. The pulse energy range in our experiment was such that ablation is always performed at values only slightly above the ablation threshold energy (for 1 pulse ablation). With our system, we can achieve depths from several tens of nanometers up to 2 micrometers by firing from 1 to 15 pulses to the same location. Deeper structures can be made by firing more than 15 pulses to the same spot. Precise depth control is a must for making diffractive optical elements (DOE). We show that depth can be controlled with a step of several tens of nanometers and that is enough for DOE fabrication.

The map of removed volume dependence on the number of pulses per spot is depicted in Fig. 8. Even while working with fluence twice higher than the ablation threshold volume removal has linear dependence and within our parameter range the ablated material volumes can be controlled from 0.15 to 17.30 μm^3.

The ablation efficiency dependence on the number of pulses and one pulse energy is depicted in Fig. 9. Efficiency values vary from 0.02 to 0.27 μm^3/μJ.

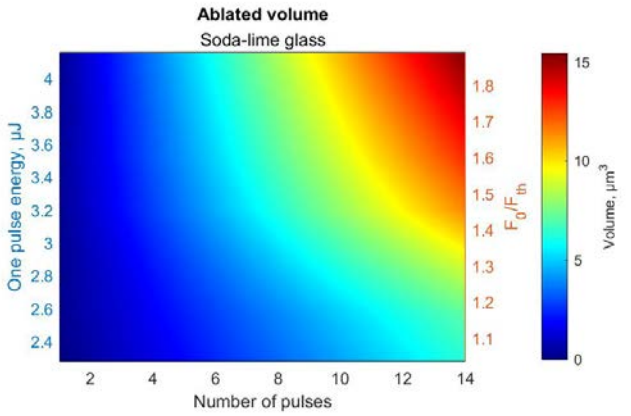

Fig. 8 Volume of the craters, ablated on soda-lime glass.

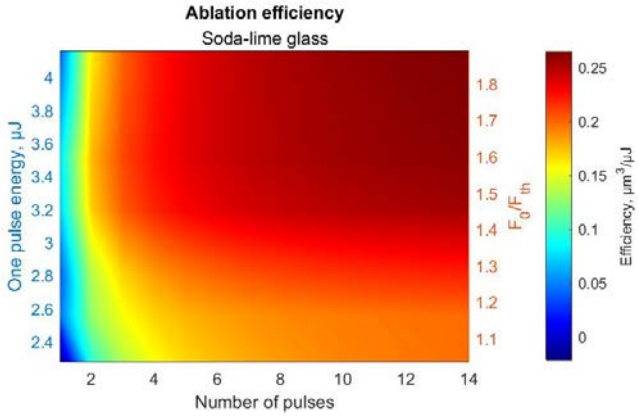

Fig. 9 Soda-lime glass ablation efficiency.

The width of the craters' dependence on the number of pulses per spot and one pulse energy is depicted in Fig. 10. Width values vary from 2 to 10 micrometers.

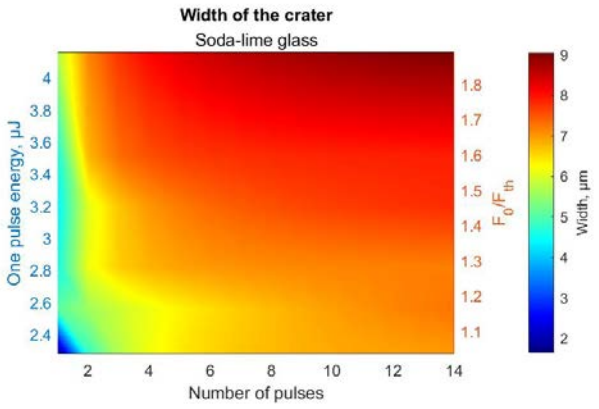

Fig. 10 Width of the craters, ablated on soda-lime glass.

For estimation of ablated craters' bottom roughness, the depth profiles were extracted from the topographic data, and waviness (crater shape) was removed by applying a 5th-order polynomial fit. Roughness values for the profiles were calculated as the arithmetical mean height (R_a). The dependencies on the number of pulses with the highest and the lowest energies are shown in Fig. 11, while Fig. 12 depicts the roughness map for all energy values. Fig. 11 shows that for the lower amount of pulses per spot the roughness dependencies on the number of pulses are comparable, however, for >6 pulses per spot lower roughness values can be achieved with a higher pulse energy.

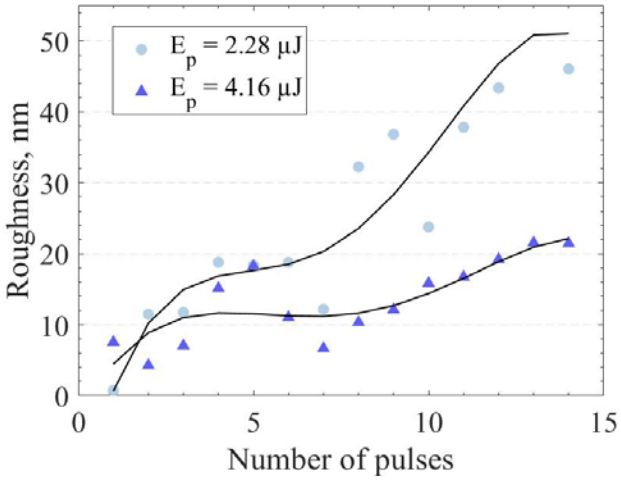

Fig. 11 Roughness dependence on the number of pulses per spot.

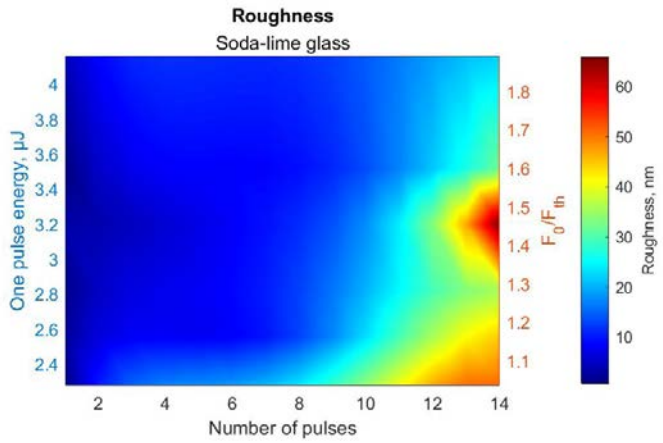

Fig. 12 Soda-lime glass ablation roughness.

The results indicate that in a wide parameter range the small roughness values (< 20 nm) could be achieved. If low pulse energies are used, nanogratings start to appear after sufficient multi-pulse processing that increases surface roughness, however, we did not observe the appearance of nanogratings with higher energies in our tested parameter range. We can speculate that further increasing the number of pulses would also lead to the formation of nanogratings. As it is shown in Fig. 12, most of our roughness results are less than 20 nm that are close to the limit resolution of Sensofar Plμ2300 profilometer (< 10 nm for high-quality mirrors) indicating that more sophisticated AFM profilometers

are required for the correct estimation of UV femtosecond laser ablated crater surfaces on dielectrics.

Ablated craters were also examined with a scanning electron microscope. SEM photos of the craters, ablated with a maximal pulse energy E_p = 4.16 μJ are depicted in Fig. 13.

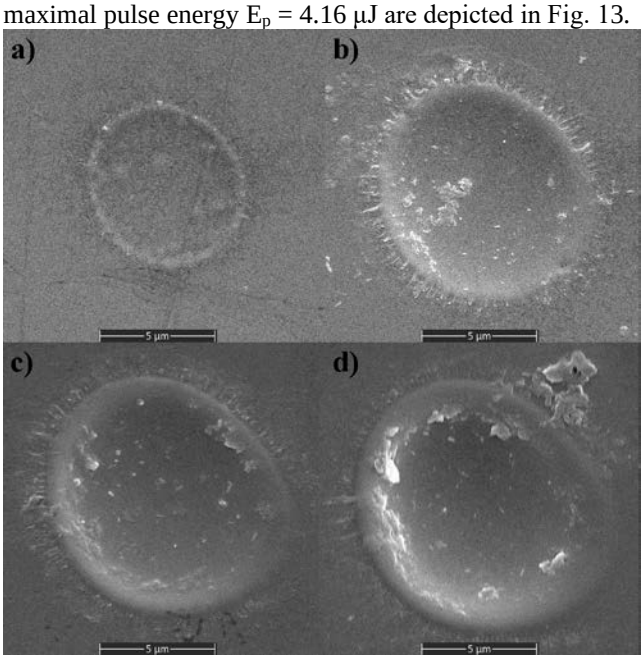

Fig. 13 Craters, ablated on soda-lime glass with a) 1, b) 5, c) 10, and d) 15 pulses per spot, E_p = 4.16 μJ.

As we can see in Fig. 13 femtosecond UV laser pulses lets to achieve a very good quality ablation with a low surface roughness of the modified zone. The dominating ablation mechanisms are vaporization and melting. As a gaussian laser pulse intensity decreases radially away from the center, the molten material also exhibits the same tendency to flow away from the center due to the pressure and resolidify. That is why some elevated material deposits on the sidewalls and thin strips are seen in SEM images (Fig. 13 – 15).

SEM photos of the craters, ablated with a minimal pulse energy E_p = 2.28 μJ are depicted in Fig. 14.

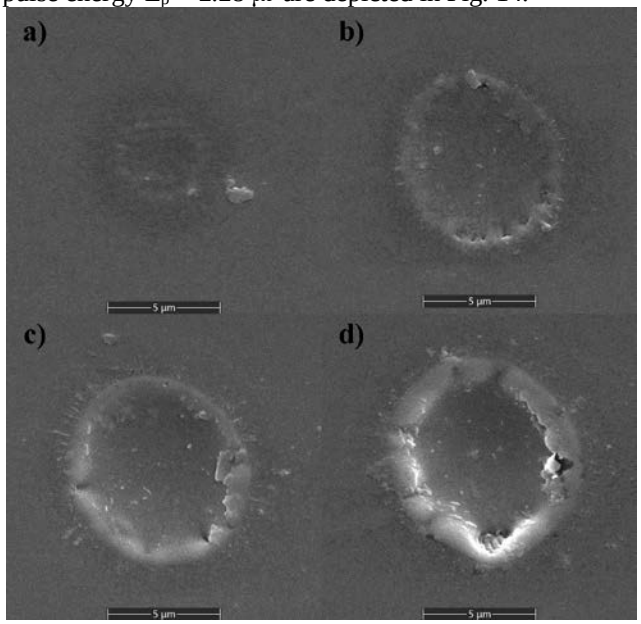

Fig. 14 Craters, ablated on soda-lime glass with a) 1, b) 5, c) 10, and d) 15 pulses per spot, E_p = 2.28 μJ.

Ablation quality if compared to Fig. 13 has reduced as nanogratings start to form on the sidewalls of the crater underneath the debris. That is because of the fluence distribution in a gaussian beam. Fluence has its maximal value in the center of a beam and reduces further from the center. If the energy is low, fluence that is further from the center is not sufficient to sustain the ablation process. If the energy would be reduced, even more, nanogratings would evolve towards the center as it is shown in Fig. 15. This crater is ablated with the energy, that is slightly below the ablation threshold (for one pulse). Ablation in this case is possible just with multiple pulses to the same spot.

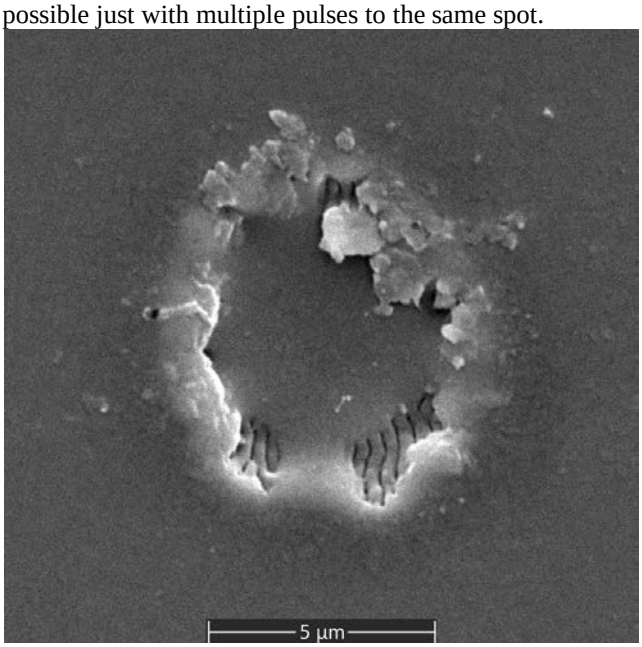

Fig. 15 Crater, ablated on soda-lime glass with 11 pulses per spot, E_p = 2 μJ.

4. Conclusions

Femtosecond UV laser ablation properties on soda-lime glass were investigated by examining craters, ablated by multiple pulses per spot. Craters' depth, width, and volume relations with several pulses per spot were calculated. The results show that in our working range depth and volume depend linearly on the number of pulses and width depends as two term power series function. The resulting energy threshold value E = 2.21 μJ, calculated by the D squared method shows, that the results are produced in the whole available parameter range – from the energy that is just slightly above the threshold value to the maximal achievable pulse energy.

Pits' width, depth, and volume parameter maps that show relations with the number of pulses per spot, laser pulse energy, and fluence are also depicted. These maps are useful when considering a working regime for the fabrication of diffractive optical elements. It's shown that with our system we can achieve depths from several tens of nanometers up to 2 micrometers and it can be controlled with a step of several tens of nanometers - that is reliable for DOE fabrication. Deeper structures can also be easily achieved by firing more than 15 pulses to the same spot.

Finally, the scanning electron microscope photos of the ablated craters prove that femtosecond UV laser pulses let

to achieve a very good quality ablation with a low surface roughness of the modified zone. Ablation quality slightly reduces for minimal pulse energy because nanogratings start forming on the crater's sidewalls, underneath the debris.

Acknowledgments and Appendixes

(1) Doc. Dr. Domas Paipulas – supervisor of the work and Ph.D. studies, who led and consulted all the work.

(2) Prof. Dr. Vytautas Jukna – consulted on "Matlab" code writing.

(3) This work has received funding from European Regional Development Fund (project No 01.2.2-LMT-K718-03-0029) under a grant agreement with the Research Council of Lithuania (LMTLT).

References

[1] M. D. Perry, B. C. Stuart, P. S. Banks, M. D. Feit, V. Yanovsky, and A. M. Rubenchik: J. Appl. Phys., 85, (1999) 6803.

[2] D. M. Karnakis, M. R. H. Knowles, K. T. Alty, M. Schlaf, and H. V. Snelling: Proc. SPIE, (2005) 5718.

[3] J. Shin, and K. Nan: Appl. Sci., 10, (2020), 987.

[4] M. E. Shaheen, J. E. Gagnon, and B. J. Fryer: Opt. Lasers Eng., 119, (2019), 18.

[5] Y.T. Chen, K. Naessens., R. Baets, Y. S. Liao, and A. A. Tseng: Opt. Rev., 12, (2005), 427.

[6] H. Liu, L. Xie, W. Lin, and M. Hong: Adv. Optical Mater., 9, (2021), 2100537.

[7] A. Saliminia, A. Proulx, and R. Vallée: Opt. Commun. 333, (2014), 133.

[8] J. R. Vázquez de Aldana, C. Méndez, and L. Roso: Opt. Express 14, (2006), 1329.

[9] H. Zhang, D. van Oosten, D. M. Krol, and J. I. Dijkhuis: Appl. Phys. Lett. 99, (2011), 231108.

[10] J. M. Liu: Opt. Lett. 7, (1982), 196.

(Received: June 26, 2022, Accepted: October 15, 2022)